European Journal of Pharmaceutical Sciences 147 (2020) 105292

Contents lists available at ScienceDirect

European Journal of Pharmaceutical Sciences

journal homepage: www.elsevier.com/locate/ejps

Mechanical properties of starch esters at particle and compact level - Comparisons and exploration of the applicability of Hiestand's equation to predict tablet strength

Nizar Al-Zoubi[a,**], Adel Ardakani[b], Faten Odeh[b], Nina Sakhnini[b], Ioannis Partheniadis[c], Ioannis Nikolakakis[c,*]

[a] Department of Pharmaceutics and Pharmaceutical Technology, Faculty of Pharmaceutical Sciences, The Hashemite University, Zarqa, 13115, Jordan
[b] Faculty of Pharmacy, Applied Science Private University, Amman, Jordan
[c] Department of Pharmaceutical Technology, School of Pharmacy, Faculty of Health Sciences, Aristotle University of Thessaloniki, Thessaloniki, 54124, Greece

ARTICLE INFO

Keywords:
Tablets
Starch esters
Surface energy
Nanoindentation
Tensile strength prediction
Hiestand's equation

ABSTRACT

Hydrophobic starch esters have potential as tablet matrix formers in controlled drug delivery. The mechanical properties of native starch (SN), starch acetate (SA) and starch propionate (SP) were studied at particle and compact level. Particle microhardness and modulus of elasticity were evaluated by nanoindentation. Force-displacement data of compressed powder were analyzed using Heckel in conjunction with piecewise regression, Kuentz-Leuenberger, Kawakita and Adams models, and yield pressure parameters were derived. Starches were characterized for chemical structure by Raman spectroscopy, crystallinity from powder x-ray diffraction (PXRD) patterns and surface energy from apparent contact angle measurements. A-type starch reflections were absent in the PXRDs of esters indicating greater amorphicity. Consequently, the particle microhardness of starch esters decreased leading to greater deformation during compaction and lower values of yield pressure parameters. These parameters increased with microhardness and ranked the starches in the order: SP < SA < SN. Fitting the experimental data into Hiestand's bonding index equation, a linear correlation (R^2 = 0.902) was established between experimental and calculated tablet strength describing results of all starches, when Adams (τ_o') yield pressure was used as the 'effective compression pressure' in the above equation.

1. Introduction

Starch is used in tablet formulations as a filler, binder and disintegrant. It receives continuous interest because of its safety, abundant availability and low cost. Chemical modification offers an approach to improve the properties of native starches, broaden functionality and enable wider pharmaceutical applications. In this context, acid modified starches from various sources have been shown be more compressible forming stronger tablets (Odeku and Picker-Freyer 2009; Akin-Ajani et al., 2014). Furthermore, hydrophobic starch esters have shown ability to form controlled release tablets by depressing swelling and enzymatic degradation (Tuovinen et al., 2004).

Several chemically modified starches have been investigated for this purpose (Ameye et al., 2001; Wöhl-Bruhn et al., 2012; Singh and Nath, 2012a, 2013a,b) with emphasis on the acetate ester (Korhonen et al., 2000; Pohja et al., 2004; van Veen et al., 2005; Mäki et al., 2006; Singh and Nath, 2012b, 2013c). Starch propionate is another ester that was recently shown to form controlled release tablets (Sakhnini et al., 2015). The controlled release ability has been related to its matrix structure, besides hydrophobicity (Korhonen et al., 2000; Sakhnini et al., 2015; Avgerinos et al., 2018). This emphasizes the importance of interparticle bonded areas and the formation of a coherent network impeding fluid penetration. Material yield pressure exerts a major influence on the extent of bonding through its effect on plastic deformation, whereas the strength of bonds is controlled by surface forces (Fichtner et al., 2008). The effects of both these factors are expressed in the value of tablet strength as highlighted in the United States Pharmacopeia Convention ⟨Chapter 1217⟩ Tablet Breaking Force (2012).

In the present study, starch propionate and starch acetate were compared to native starch in terms of yield pressure parameters derived from compression models. The Heckel model is sensitive to materials

* Corresponding author.
** Corresponding author.
E-mail addresses: nzoubi@hu.edu.jo (N. Al-Zoubi), yannikos@pharm.auth.gr (I. Nikolakakis).

https://doi.org/10.1016/j.ejps.2020.105292
Received 3 August 2019; Received in revised form 20 January 2020; Accepted 2 March 2020
Available online 07 March 2020

and the composition but when represented graphically it deviates from the assumed linearity necessitating selection of a compression range for the computations (Patel et al., 2010; Cespi et al., 2014). Kuentz and Leuenberger (1998) extended this model by expressing the dependence of deformation on compression pressure as a hyperbolic function, the constants of which were incorporated into the equation. Their model was able to distinguish lactose plastic properties more effectively than Heckel's model due to better accuracy (Lamešić et al., 2018, Paul and Sun 2017). Kawakita's model (Kawakita and Lüdde, 1971) also includes a parameter related to the yield stress of compacted powder and generally shows good linearity. Adams and co-workers extended the last model and obtained good correlations between yield pressure of compacted powder and single agglomerate strength (Adams et al., 1996).

Furthermore, particle microhardness, of the native and esterified starches was examined, since it is a fundamental property correlating with material plasticity and has been proposed for screening compaction performance (Yap et al., 2008, Cao et al., 2010, Govedarica et al., 2012). So far, correlation between hardness and powder compaction parameters has been established (Cao et al 2010, Govedarica et al. 2012) and there is one work reporting correlation between microhardness and tablet strength, but for a given material (Sun et al., 2018). There is no general correlation, which is ascribed to the variability of tested particles (size, shape, crystal form, exposed crystal plane, surface homogeneity), differences in the experimental conditions (sample preparation, instrumentation, operation) and different interparticle forces and interactions (Feng et al. 2007, Picker-Freyer et al., 2007, Masterson and Cao, 2008).

The objective of this work was two-fold. i) to compare the native and esterified starches at particle and compact level using nanoindentation and powder compression models and elucidate relationships between the different measurements. ii) to examine possible correlations between experimental and calculated tensile strength on the basis of Hiestand's bonding index equation (1985) which takes into account particle size, microhardness, 'effective compression pressure', number of interparticle contacts (co-ordination number) and dispersive surface forces. The ultimate purpose was to develop a tablet strength equation representing all three starch powders.

2. Materials and methods

2.1. Materials

Native maize starch (SN) was purchased from GCC Gainland Chemical Company (Clwyd, UK). Starch acetate (SA) and starch propionate (SP), with degree of substitution (DS) = 2.0, were synthesized by partially reacting hydroxyl groups of starch chains with acetic acid anhydride or propionic acid anhydride as previously described (Sakhnini et al., 2015).

2.2. Particle size, density and water content

Particle size of the experimental powders was estimated with optical microscopy and image analysis system using an Olympus BX41 microscope fitted with upper single port and camera image adapter (U-SPT and U-PMTVC) extensions (Olympus Corporation, Tokyo, Japan), Leica DF295 video camera (Leica, Germany), and Leica Microsystems software (Leica, Switzerland). About 300 particles were analyzed in different fields and mean particle size was expressed as equivalent circle diameter. Particle density (ρ_S) was determined with helium pycnometry (Ultrapycnometer 1000, Quantachrome Instruments, Boynton, USA). The volume of accurately weighed samples (average of 5 runs) was measured after calibration with a standard 7.0699 cm^3 steel ball. The amount of moisture that may be released during the density measurement can lead to errors in measured true density (Sun, 2004). For this reason, successive measurements of the same sample were made which showed differences only in the third decimal (no significant weight change) and hence there is no moisture release.

Water content was measured by thermogravimetry using a TGA−50 analyzer connected to a TA-60-WS controller (Shimadzu Corporation, Kyoto, Japan). Water content was controlled by keeping test samples in desiccators over K_2CO_3 (RH% ~43%) prior to experimentation and in similar environmental conditions during compression and mechanical testing, using a dehumidifying unit (Pretema AG, Zurich Switzerland). During nanoindentation test RH% was checked and was ~40%.

2.3. Raman spectroscopy

A Cora 5600 (Anton Paar, Graz, Austria) equipped with an optical wave guiding fiber probe was used to obtain Raman spectra at 785 nm excitation wavelength. The instrument was calibrated with a benzonitrile standard. Samples were filled in standard glass vials and the optical fiber probe was placed at 5 mm distance from the sample. The laser power was 450 mW and the acquisition time 1000 ms. The average of 10 collected spectra was taken. A dark background was acquired for each experiment and subtracted from the data to remove signals from ambient light and detector dark current.

2.4. Powder X-ray diffraction (PXRD)

Changes in the crystallographic characteristics of the starches were examined using a Rigaku Ultima IV diffractometer (Tokyo, Japan) fitted with a Cu anode at 40 kV and 40 mA. Samples were scanned from 3° to 50° 2-theta at a speed of 4° min^{-1}. The solid-state changes due to esterification were examined on the basis of the reflections present and their intensity by comparing the measured PXRD with published data.

2.5. Scanning electron microscopy (SEM)

The morphology of the surface of tablets was examined by Field Emission Gun scanning electron microscopy (FEI Company – Inspect F50/FEG, Eindhoven, Netherlands). Samples were mounted on aluminum stubs with double-sided sticky discs of conductive carbon and then coated with ~15 nm of platinum in a sputter coater (Emitech K550X, Ashford, Kent, UK).

2.6. Free energy characteristics

The surface free energies γ_s of the three starch powders were obtained from contact angle measurements using distilled water saturated with starch powder and methylene iodide (analytical grade, Aldrich, Germany) as test liquids and a cathetometer for measuring the drop height. Liquid was added dropwise from a 10 ml burette to the surface of compacted powder. Height was recorded continuously with 0.3 μm accuracy using LVDT transducer connected to a signal conditioner (E309, RDP Electronics, UK) and data acquisition unit (Handyscope TiePie Electronics, The Netherlands) by moving the horizontal telescope so that the crosshair in the eyepiece coincided with the top of the drop. Contact angle (θ) was determined from the maximum drop height according to Eq. (1) (Heertjes and Kossen, 1967, Lerk et al., 1976).

$$cos\theta = 1 - \sqrt{\frac{(Bh2)}{3\rho_F\left(1-\left(\frac{Bh2}{2}\right)\right)}} \quad (1)$$

h is the height of liquid drop, ρ_F the solid fraction of compressed powder and $B = \rho_L{*}g/2\gamma_L$ (ρ_L liquid density, g acceleration due to gravity and γ_L surface tension of liquid).

The dispersive (γ_S^d) and polar (γ_S^p) components of the surface free energy (γ_S) of each starch were calculated from the equation of Wu (1971):

$$\gamma_{LS} = \gamma_L + \gamma_S - \frac{4\gamma_L^d \times 4\gamma_S^d}{\gamma_L^d + 4\gamma_S^d} - \frac{4\gamma_L^p \times 4\gamma_S^p}{\gamma_L^p + 4\gamma_S^p} \quad (2)$$

after replacing the interfacial free energy (γ_{LS}) according to Young-Dupré Eq. (3).

$$\gamma_{LS} = \gamma_S - \gamma_L \times cos\theta \quad (3)$$

The values of γ_S^d and γ_S^p were computed by applying non-linear multiple regression to three replicated apparent contact angles measured for each starch – test liquid (Zografi and Tam, 1976). 22.1 and 50.7 mN/m were the dispersive (γ_L^d) and polar (γ_L^p) surface energy components for distilled water, and 44.1 and 6.7 mN/m for methylene iodide.

2.7. Nanoindentation

The microhardness of starches was measured at 24 °C and 40% relative humidity using an Ultra Nanoindentation Tester (UNHT, Anton Paar, Austria) fitted with a Berkovich indenter according to the method of Oliver and Pharr (2004). Samples were dissolved in isopropanol and a drop was placed on a glass slide, leaving after evaporation particles stuck to the surface. The test consisted of three phases: application of 0.5 mN load, holding for 10 s and unloading. Force during loading/unloading was applied at 1.5 mN/min. From about 30 measurements performed on each starch, 17 useable force-displacement curves were processed.

Hardness (H) was estimated by fitting Eq. (4) to the upper part of the unloading force-displacement curves (see Oliver and Pharr, 2004) where F the applied load, h the indentation depth under F, h_p the permanent indentation depth after force removal and h_{max} the depth at F_{max}.

$$F = F_{max}\left(\frac{h - h_p}{h_{max} - h_p}\right)^m \quad (4)$$

The exponent m was found by regression analysis and substituted into Eq. (5) to give the contact stiffness S from which the depth h_r corresponding to the intersection of the tangent at F_{max} with the penetration depth axis was obtained using Eq (6). Finally, the depth h_c where the indenter tip is in contact with the sample at F_{max} was obtained from Eq. (7), and from this the contact area A_p and the indentation hardness using Eq. (8).

$$S = m\left(\frac{F_{max}}{h_{max} - hr}\right) \quad (5)$$

$$h_r = h_{max} - \left(\frac{F_{max}}{S}\right) \quad (6)$$

$$h_c = h_{max} - \varepsilon(h_{max} - h_r) \quad (7)$$

$$H = \frac{F_{max}}{A_p} \quad (8)$$

Furthermore, the Young's modulus E was calculated from Eqs. (9) and (10)

$$E_r = \frac{\sqrt{\pi}.\,S}{2.07\sqrt{Ap}} \quad (9)$$

$$\frac{1 - \nu_s^2}{E} = \frac{1}{E_r} - \frac{1 - \nu_i^2}{E_i} \quad (10)$$

where ν_s is the Poisson's ratio of the starch powder, and ν_i, E_i constants of the indenter.

2.8. Powder compaction and compression models

A fixed 70 mg amount of each powder was compressed on an instrumented tablet press (Model GTP-1, Gamlen Tableting Ltd, Nottingham, UK) fitted with 6-mm flat-faced punches and operated at 10 mm/min speed in the pressure range 69-174 MPa. Force-displacement profiles were recorded at 200 Hz frequency.

The punch position was corrected for elastic deformation using Eq. (11) ($R^2 = 0.997$)

$$\delta x = 8.0F10^{-4} - 6.8F^2 10^{-7} \quad (11)$$

where δx the change of punch position (mm) during compression in empty die and F is the compression force applied in kg.

Elastic recovery (ER%) was expressed as the %increase in tablet thickness after compression pressure removal ($P = 0$) compared with that at 174 MPa compression.

2.8.1. Heckel model

This model is expressed by Eq. (12) where the reciprocal slope 1/K is the yield pressure (Py) or the ability of the material to deform plastically.

$$ln\left[\frac{1}{(1 - p_F)}\right] = A + KP \quad (12)$$

The left part of the equation is a densification function. P is the compression pressure, p_F the solid fraction [= compact weight/(volume × particle density)] and A the intercept related to volume reduction due to die filling and particle rearrangement before compaction. The solid fraction p_{FA} where the linear part of Heckel plot intercepts the densification axis is obtained from Eq. (13) and represents the onset of compaction.

$$p_{FA} = 1 - e^{-A} \quad (13)$$

Heckel model was originally derived for plastic metal powders where after an initial curved part the plot becomes linear (Heckel 1961, Fig. 4 in his paper). In the compaction of pharmaceutical powders other factors such as fragmentation and elasticity are involved causing deviations from linearity not only at low but at higher pressures as well (Adams and McKeown 1996). In general, the curvilinear plot can be considered as being composed of three sequential regions of initial packing, plastic deformation and an elastic/hardening region (Roberts and Rowe, 1987; Nyström et al., 1993). The intermediate plastic region is used to find p_{Fa} and Py. The three regions can be distinguished by piecewise regression, represented by a continuous line with two break points, as shown graphically in Fig. 1 for native starch. The two breaks divide the line in three regions: the first begins at the beginning of packing, point y_o/p_o, (y value on densification axis and p on pressure axis) and ends at the first break point y_1/p_1' corresponding to the beginning of plastic deformation; the second begins from the first break point and ends at the second y_2/p_2' corresponding to the end of

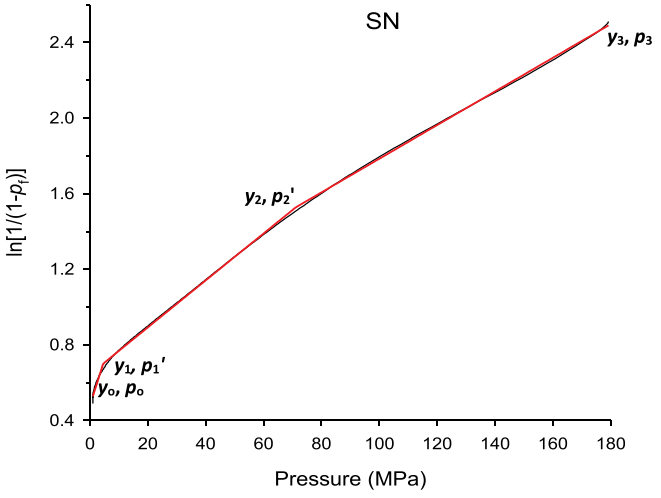

Fig. 1. Fitting of piecewise regression continuous line with two break points to the Heckel plot of native starch

Table 1
Particle density, size, shape, microhardness and elastic modulus for native starch and starch esters.

Starch type	Particle density (g/cc)	Particle size distribution				Shape index	Moisture content (%)	Micro-hardness (MPa)	Elastic modulus (GPa)
		D_{10} (μm)	D_{50} (μm)	D_{90} (μm)	D_{90}/D_{10}				
SN	1.52	12.3	13.9	17.2	1.4	1.17	9.8 ± 0.2	238.6 ± 92.1	3.9 ± 1.3
SA	1.37	10.8	18.6	32.8	3.0	1.86	2.6 ± 0.1	87.4 ± 44.7	2.1 ± 0.6
SP	1.34	11.4	18.2	27.1	2.4	1.65	6.3 ± 0.1	41.4 ± 34.0	1.5 ± 1.0

SN: Native starch; SA: Starch acetate; SP: Starch propionate.

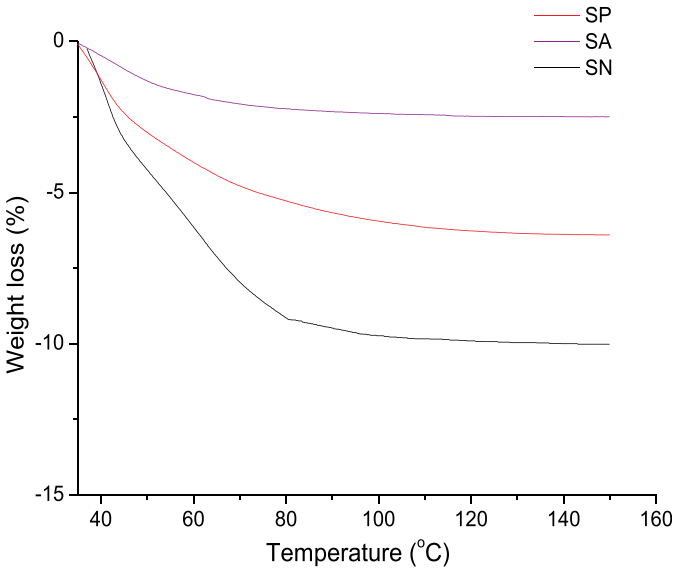

Fig. 2. Thermograms showing loss of water content for native starch (SN), starch acetate (SA) and starch propionate (SP)

plastic and beginning of predominantly elastic deformation; the third region begins from the second break point and ends at point y_3/p_3 of maximum pressure. The above three ranges are described by the following equations.

$$f(1) = [y_0(p_1' - p) + y_1(p - p_1)]/(p_1' - p_1) \text{where} \, p_1 < p \le p_1' \quad (14i)$$

$$f(2) = [y_1(p_2' - p) + y_2(p - p_1')]/(p_2' - p_1') \text{where} \, p_1' < p \le p_2' \quad (14ii)$$

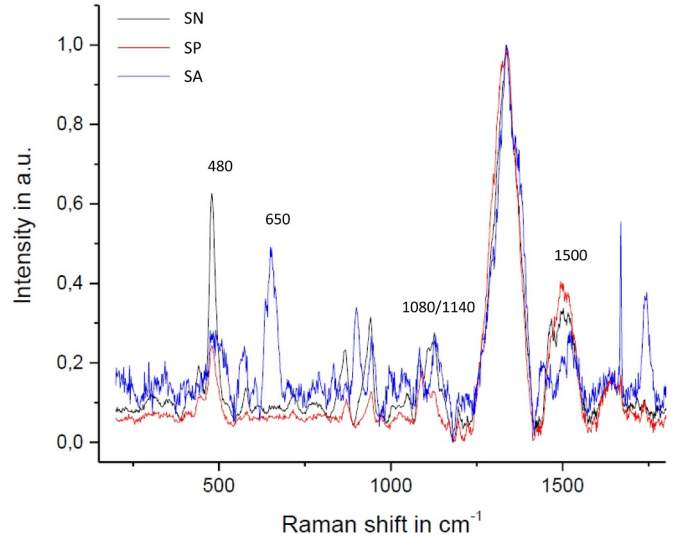

Fig. 3. Raman spectra for native starch (SN), starch acetate (SA) and starch propionate (SP).

$$f(3) = [y_2(p_3 - p) + y_3(p - p_2')]/(p_3 - p_2') \text{where} \, (p_2' < p \le p_3) \quad (14iii)$$

The break points were obtained by regression analysis (SigmaPlot 11.0, Systat, Inc.).

2.8.2. Kuentz-Leuenberger model

This model (abbreviated K-L) is described by Eq. (15) where C_{KL} and p_{FC} are constants determined by plotting the differential dp_F/dP against p_F and fitting the hyperbolic Eq. (16) to the data. It is a modification of the Heckel Eq. (11) where the pressure susceptibility parameter $(dp_F/dP)/(1\text{-}p_F)$ is used instead of constant K. It has been found to fit well the compressibility out-of-die data for polymeric powders and be more accurate (Kuentz and Leuenberger 1999, Paul and Sun, 2017).

$$P = 1/C_{KL}\left[p_{Fc} - p_F - (1 - p_{Fc})\ln\left[\frac{(1 - p_F)}{(1 - p_{Fc})}\right]\right] \quad (15)$$

$$\frac{dp_F}{dP} = \frac{C_{KL}}{(p_F - p_{Fc})} \quad (16)$$

C_{KL} represents plasticity, and hence $1/C_{KL}$ can be considered as yield pressure. p_{FC} is the solid fraction at which the powder bed attains mechanical rigidity (Kuentz and Leuenberger, 1999).

2.8.3. Kawakita model

This model is expressed by Eq. (17) where C is the degree of volume reduction

$$\frac{P}{C} = \frac{P}{a} + \frac{1}{ab} \quad (17)$$

$$C = \frac{(V_o - V)}{V_o} \quad (18)$$

V_O is the initial volume, V volume at pressure P, and a, b constants obtained from the slope and the intercept of the P/C vs P plot. Constant 'a' is related to maximum volume reduction or the compressibility of

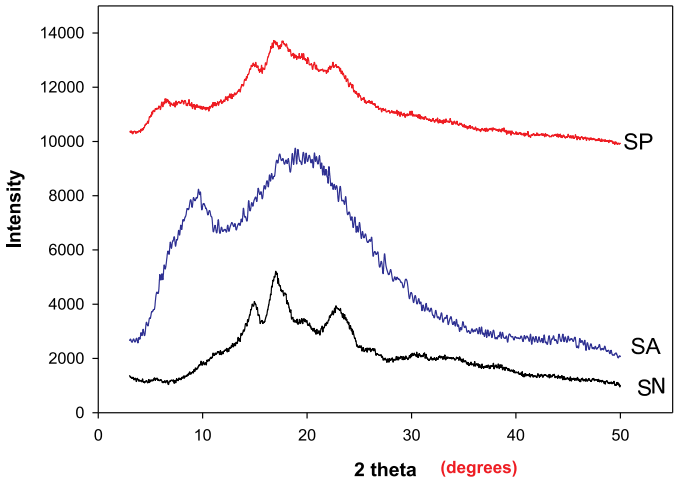

Fig. 4. PXRD patterns for native starch (SN), starch acetate (SA) and starch propionate (SP).

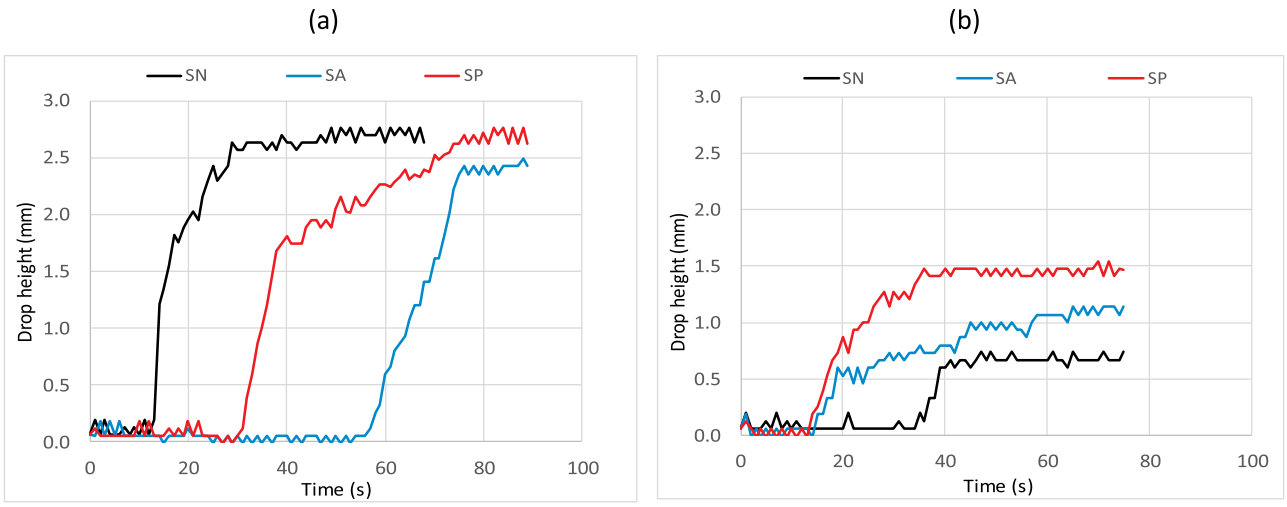

Fig. 5. Recordings of drop height during dropwise addition of (a) water and (b) methylene iodide. On the surface of compacts of native starch and starch esters.

Table 2
Determination of surface energy from dynamic contact angle measurements (mean ± sd).

Starch type	Water		Methylene iodide		Surface energy components		
	Droplet height (mm)	Contact angle (θO)	Droplet height (mm)	Contact angle (θ^O)	γ_s^d (%γ_s)*	γ_s^p (%γ_s)*	γ_s
SN	2.50 ± 0.10	58.0 ± 1.6	0.50 ± 0.07	36.4 ± 3.2	29.8 (57.9%)	21.6 (41.9%)	51.5
SA	2.24 ± 0.06	54.5 ± 0.9	0.85 ± 0.04	47.1 ± 1.4	25.2 (49.7%)	25.6 (50.5%)	50.7
SP	2.64 ± 0.04	59.2 ± 0.8	1.40 ± 0.06	65.3 ± 2.2	17.7 (39.4%)	27.2 (60.6%)	44.9

* γ_{sd}, γ_{sp} are dispersive and polar components respectively of surface energy. Values in parentheses express percentages of total surface energy γ_s

the powder and $1/b$ is considered a measure of yield pressure of particles (Adams and McKeown 1996). The application of the model is straightforward and was originally proposed for application to the compression of soft, fluffy powders at low porosities. Its overall ability to fit compression data has been criticized by Denny (2002).

2.8.4. Adams model

This model is expressed by Eq. (19) where τ_o' is the apparent particle strength, α' the apparent coefficient of friction and ε_n equals $\ln(h_i/h_p)$ where h_i is the initial height of the powder bed and h_p the height at pressure P. It represents a fundamental approach to compression since τ_o' is proportional to the single particle-agglomerate crushing load and α' is related to frictional forces. However, it assumes completely dissipative system, i.e. negligible storage of elastic energy.

$$lnP = \ln\left(\frac{\tau_o'}{a'}\right) + a'\varepsilon_n + \ln\left[1 - e^{(-a'\varepsilon_n)}\right] \tag{19}$$

2.9. Experimental and calculated tablet tensile strength

The breaking force (F) under diametrical tablet compression was measured 72 h after compaction with the tablet press described above (Model GTP-1, Gamlen Tableting Ltd) but operated in fracture mode. Tablet dimensions were measured with a digital Vernier caliper with 0.01 mm resolution (Mitutoyo, Kawasaki, Japan). Tensile strength (σ_T) was calculated from Eq. (20) (Fell and Newton, 1970) where d the diameter of the tablet and t its thickness.

$$\sigma_T = \frac{2F}{\pi dt} \tag{20}$$

Calculation-prediction of tensile strength was made on the basis of the bonding index Eq. (21) (Hiestand, 1985). For solid fractions $\rho_F \geq 0.74$ it takes the form

$$\sigma_T = \frac{P'\gamma^d}{\xi_i r}\left[\frac{N\varphi}{(2-\rho_F)P'H}\right]^{0.5} \tag{21}$$

where σ_T is the tablet tensile strength (MPa), P' the 'effective compression pressure' for particle deformation, expressed as one of the four compression model yield pressure parameters, γ^d the dispersive component of surface energy, H the particle microhardness, r its radius (μm) and φ is a correction factor for the effect of orientation taken as 1. ξi is the strain index [$=H^*(1-\nu^2)/E$] where E the Young's modulus obtained from Eq. (10) and ν the Poisson's ratio taken as 0.3. The value of the coordination number N suggested by Hiestand is 3 but other values have also been used to give better prediction (Ouchiyama and Tanaka 1981; Nikolakakis and Pilpel 1988). For the construction of the graphs and non-linear fitting SigmaPlot 11.0 software (Systat, Inc.) was used.

3. Results and discussion

3.1. Particle, density and moisture content

Table 1 presents results of particle density and particle size distribution for the studied starch powders expressed as percentage of particles finer than 10% (D_{10}), 50% (D_{50}) and 90% (D_{90}). The starch esters (acetate, SA and propionate, SP) had slightly bigger particles than native starch (SN) (D_{50} 18.6 and 17.9 μm compared to 13.9 μm) and slightly wider size distribution (D_{90}/D_{10} 3.0 and 2.4 compared to 1.4), while their particle densities were slightly lower due to the presence of the lower density acetyl or propionyl moieties in the molecule. Results of thermogravimetry and water loss are presented in Fig. 2. From the three thermograms it appears that native and esterified starches had different water contents of 9.8%, 2.6% and 6.3% for SN, SA and SP respectively. It is also noticed that a significant percentage is lost at low temperatures of about 40-45 °C, corresponding to externally adsorbed water (Malamataris et al., 1991).

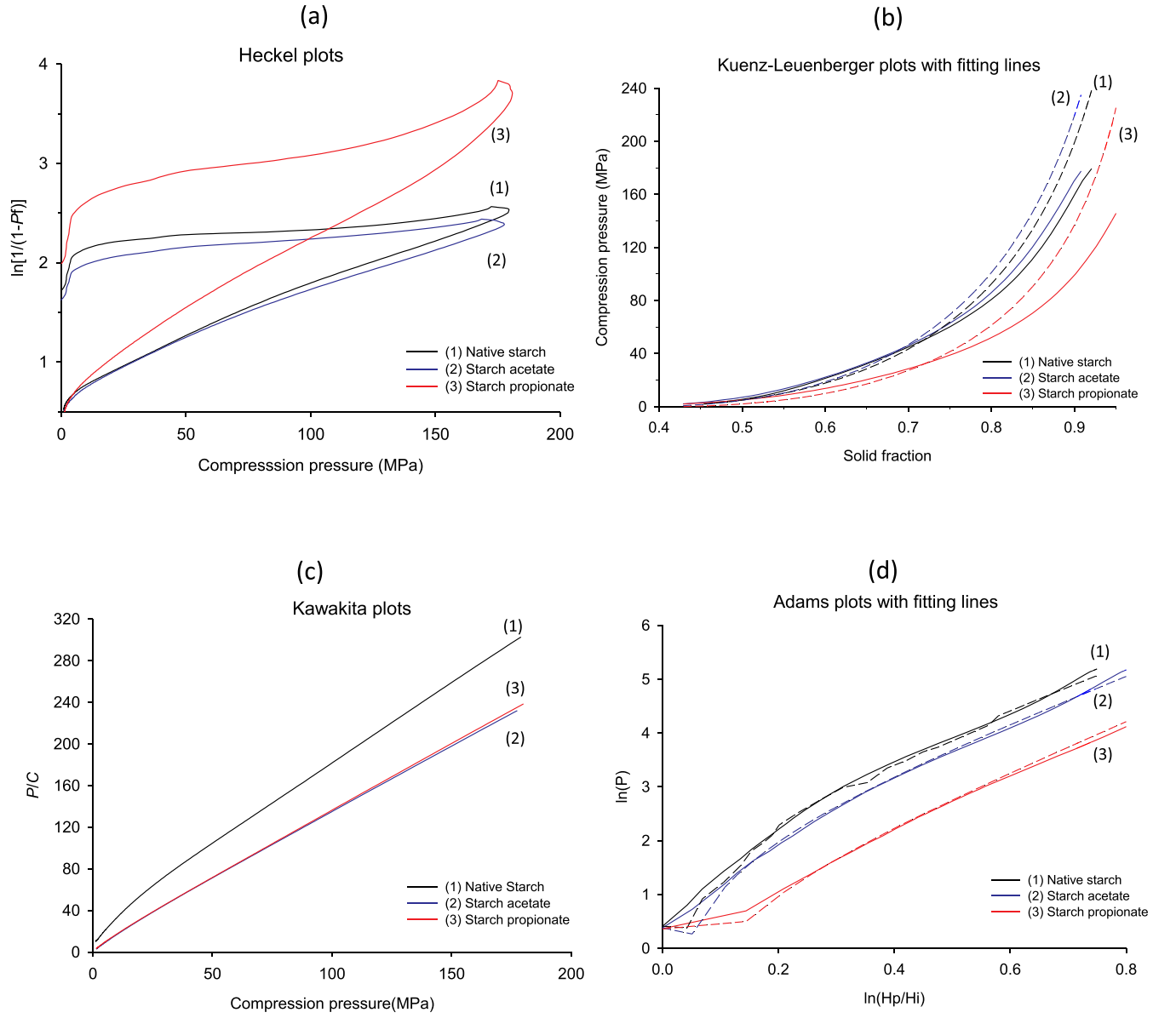

Fig. 6. Compression plots according to Heckel (a), Kuentz-Leuenberger (b), Kawakita (c) and Adams (d) models.

Table 3
Densification parameters and yield pressures at the end points of the 3 compression regions defined by piecewise regression analysis of Heckel plots.

Starch type	Piecewise regression analysis				
	y_o/p_o	y_1/p_1'	y_2/p_2'	y_3/p_3	R^2
SN	0.527/1.3	0.701/6.5	1.513/71.4	2.498/174.0	0.999
SA	0.548/2.3	0.751/10.2	1.411/65.3	2.368/174.0	0.999
SP	0.567/2.0	1.112/25.1	3.182/163.1	3.662/174.0	0.998

y_o, p_o are densification function $\ln[1/(1-p_F)]$ and compression pressure respectively at the beginning of packing, y_1, p_1' values at the end of the packing and beginning of the compaction region, y_2, p_2' values at the end of compaction and beginning of the elastic region, and y_3, p_3 values at maximum pressure.

3.2. Raman spectroscopy

Fig. 3 presents Raman spectra. The spectral signature of native starch (SN) appears to be in good agreement with the peaks reported in literature (Almeida et al., 2010). Within the analyzed fingerprint region, the peak at 480 cm^{-1} can be assigned to C—C—C bending and C—O torsion modes. The band between 1 080 and 1 140 cm^{-1} originates from C—O and C—C stretching vibrations as well as C—O—H bending vibrations. The most prominent peak centered at 1336 cm^{-1} is caused by C—O stretching and C—O—H bending vibrations. The spectrum of starch acetate (SA) shows strong vibrations at 650 cm^{-1} due to the O—C—O angular deformation mode besides the peaks of SN (Pereira et al., 2006). Signals at 900 cm^{-1}, 1 669 cm^{-1} and 1 740 cm^{-1} cannot be easily assigned. The spectrum of starch propionate (SP) is similar to SN. A higher intensity peak due to ester modification is only seen at 1 500 cm^{-1} (CH, CH_2 and C—O—H bending).

3.3. Crystallinity

PXRD patterns were acquired to identify changes in crystallinity due to esterification. These are presented in Fig. 4. The pattern of SN shows strong, relatively sharp reflections around 2-theta 15.00° and 17.00° and at 22.75° indicating A-type crystal structure. The replacement of about two thirds of hydroxyl groups by acetate or propionate groups led to disruption of crystallinity, manifested in the PXRDs as reduction of

Table 4
Yield pressure parameters and model constants derived from the Heckel, Kuentz-Leuenberger, Kawakita and Adams powder compression models.

Starch type	Heckel			Kuentz-Leuenberger			Kawakita			Adams		
	p_{FA}*	*Py* (MPa)	R^2	p_{FC}*	$1/C_{KL}$ (MPa)	R^2	a*	$1/b$ (MPa)	R^2	α'	τ_o' (MPa)	R^2
SN	0.479 ± 0.04	82.6 ± 1.8	0.999	0.372 ± 0.05	358.6 ± 10.7	0.891	0.64 < 0.01	16.4 ± 0.8	0.996	4.10 ± 0.3	31.6 ± 0.6	0.993
SA	0.474 ± 0.03	82.0 ± ± 1.1	0.998	0.381 ± 0.05	316.3 ± 4.5	0.736	0.78 < 0.01	6.3 ± 0.3	0.999	4.27 ± 0.1	22.8 ± 0.4	0.993
SP	0.556 ± 0.02	69.9 ± ± 0.8	0.998	0.410 ± 0.04	242.3 ± 8.9	0.839	0.78 < 0.01	5.7 ± 0.1	0.999	4.60 ± 0.1	8.1 ± 0.1	0.993

p_{FA}, p_{FC} are the solid fraction at the onset of compact formation, a Kawakita's compressibility parameter and α' the apparent coefficient of friction.

the intensity or absence of the characteristic reflections of A-type structure and the appearance of broad ones at 2-theta between 5° and 10° (Zhu et al., 2007; Diop et al., 2011; Hong et al., 2015). These changes indicate reduction of crystallinity and perhaps partial change of crystal structure from A- to B- type (Buléon et al., 1998).

3.4. Surface energy

From the various techniques that can be applied to characterize the surface of polymers of natural origin, wetting techniques are preferred as being more sensitive to chemical heterogeneity (Heng et al., 2007). However, morphological heterogeneity is a source of variation in contact angle measurement. For this reason, the term 'apparent' contact angle is used, related to the inability to correct for false assumptions of perfectly smooth surface and non-absorbing material. That the values are not absolute is irrelevant to this work, as the need is to know how liquid interacts with the compact. To minimize errors, measurements were made on plastically deformed tablets compressed at maximum pressure (174 MPa), since they present smoother surface and provide consistent values reflecting better the surface energy (Buckton and Newton 1986, Holm et al 2016). It is also expected, that due to the low compact porosity and the use of saturated test solutions, water absorption and swelling and effects are reduced.

Fig. 5 presents the increase of drop height formed on the surface of compacts during dropwise addition of test liquids. The drop height is seen to increase in a slip-stick manner which is ascribed to surface heterogeneity (Kung et al., 2019). Table 2 lists the measured drop heights and derived apparent contact angles together with the dispersive and polar components of surface energy. For water, the drop height and θ are similar for SN and SP but smaller for SA, whereas for methylene iodide (Fig. 5b), they are all different, increasing in the order SN < SA < SP.

From the θ values, the dispersive and polar components of the surface energy of the three starches were derived (Table 2). The dispersive component γ_s^d increases in the order SP < SA < SN whereas the polar component γ_s^p in the order SN < SA < SP. Starch is known to consist of amylopectin (about 70–80%) and amylose (20–30%) organized in lamellae. In these structures, they are arranged in double helix strands positioned perpendicular to the particle surface, leading to uneven distribution of chemical groups between the surface and particle interior (Raatikainen et al., 2002; Perez and Bertoft, 2010). Therefore, esterification may have caused higher concentration of acetate or propionate groups at the surface, resulting in greater surface polarity.

3.5. Particle microhardness

Table 1 presents results of particle microhardness and elastic modulus. The esters have considerably lower microhardness (87.4 and 41.4 compared to 238.6 MPa) and elastic modulus (2.1 and 1.5 compared to 3.9 GPa) which can be attributed to the loss of crystallinity due to esterification. The lower microhardness of the propionate than the acetate ester can be explained by its greater structure relaxation or less coherent structure (Yang and Montgomery, 2008).

3.6. Compression models

The analysis of compression models is important for understanding the compaction process, since it provides information about the powder resistance or plastic deformation during compaction and about the critical solid fraction at which the powder transforms into a compact. In Fig. 6, plots of Heckel, K-L, Kawakita and Adams models constructed according to Eqs. (12), (17), (15), (19) are presented. The dotted lines in K-L and Adams plots Fig. 6b, d) are fittings of Eqs. (15) and ((19). Overall, the positions of the curves in each subfigure are different, and hence the models are able to distinguish their compression behavior. In Table 3 results of the piecewise regression applied to identify the plastic deformation region in Heckel plots are shown. For all starches the fitting was good ($R^2 > 0.998$).

Derived parameters for the four models are presented in Table 4. Except K-L, for all starches the other models fitted the data well ($R^2 > 0.993$). K-L model fitted the data only up to solid fraction of about 0.7 (Fig. 6b), resulting in poor overall fitting ($R^2 = 0.891$, 0.736 and 0.839 for SN, SA and SP, Table 4). Therefore, the parameters $1/C_{KL}$ and p_{FC} do not represent the entire compaction process. The poor fitting of data by K-L at higher pressures is because of the greater contribution by elastic deformation to overall tablet porosity. This effect is particularly large for elastic materials such as starch. Therefore, the difference of these results from Kuentz-Leuenberger (1999) is mainly ascribed to the different method applied for the study of compaction, i.e 'in-die' in the present work vs 'out-of-die' used by the above investigators

From Fig. 6a it can be seen that Heckel plots show pronounced deviations from linearity at low pressures due to particle rearrangement, and in the case of the propionate ester also at high pressures. The continued increase of densification after force removal implies viscoelastic behavior. Comparing the Heckel (p_{FA}) and K-L (p_{FC}) packing parameters in Table 4, it appears that the former for all starches has higher values representing beginning of compact formation, whereas the latter represents transition of the powder to a mechanically stable structure (Kuentz and Leuenberger, 1999). Both parameters have similar values for SN, SA but greater for SP. Kawakita's compressibility (a'), is higher for the esters compared to native starch. Adams apparent friction coefficient' (α') increases in the order SN < SA < SP implying increase of frictional forces during compaction as microhardness decreases (Table 1).

Turning to the parameters expressing yield pressure, it appears from Table 4 that for all starches, *Py*, $1/C_{kl}$, 1/b, τ_o' follow a similar trend, i.e. their values are greater for SN (82.6, 358.6, 16.4 and 31.6 MPa respectively), followed by SA (82.0, 316.3, 6.3 and 22.8 MPa) and SP (69.9, 242.3, 5.7 and 8.1 MPa). The value 82.6 MPa of Heckel *Py* for native starch is about twice than 40.3 MPa reported by Roberts and Rowe (1987). Since our compaction speed was greater (3 mm/s instead of 0.033 mm/s Fig. 1 in their paper) and since for starch the dependence of *Py* on compaction speed (strain rate sensitivity, SRS) is well-

known (Katz and Buchner 2013), the difference should be mainly due to the compaction speed. Using SRS = 100% (Fig. 1 in Robert and Rowe paper), their *Py* value becomes 80.6 MPa, showing good agreement with 82.6 MPa of this work. This provides support for the use of piecewise regression as a method for selecting the plastic deformation region in Heckel plots.

Overall, the above results provide clear evidence of the greater plasticity of the esterified over native starch and of propionate over the acetate ester.

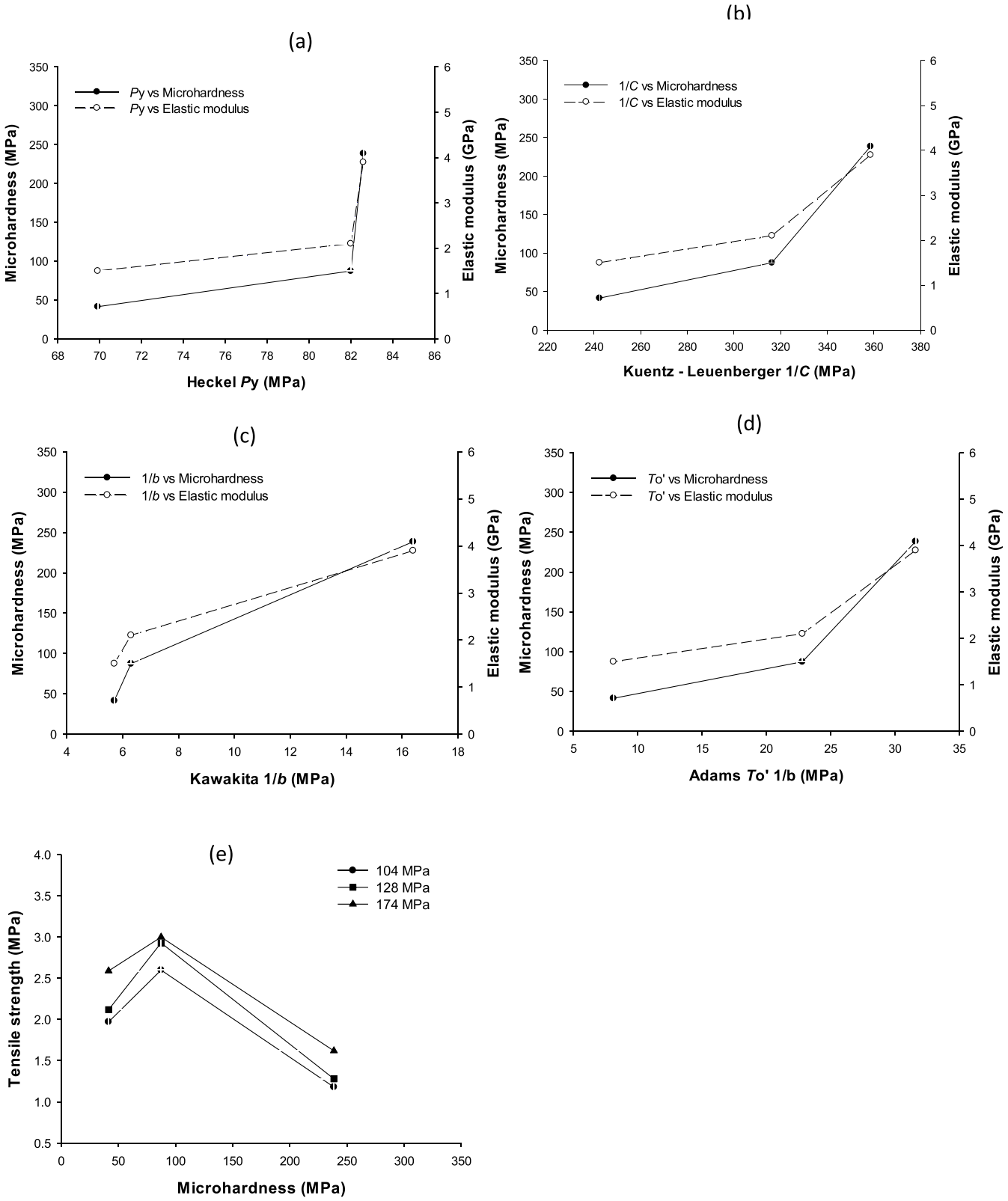

Fig. 7. Plots of microhardness of starch powders against yield pressure parameters of: (a) Heckel, (b) K-L, (c) Kawakita and (d) Adams and plot of tablet strength against microhardness (e) for tablets prepared at different compressions.

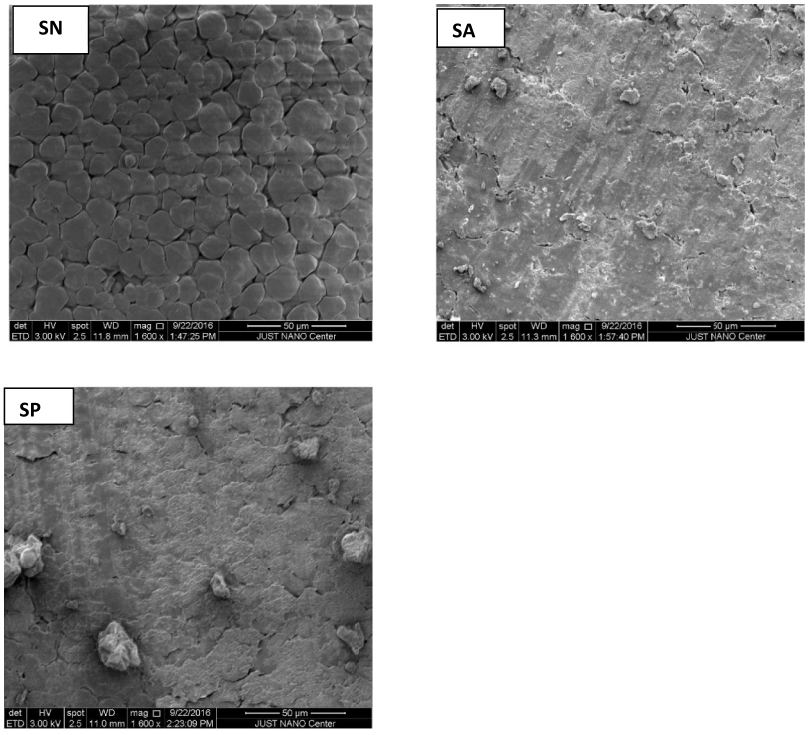

Fig. 8. SEM photomicrographs of the upper surface of tablets of native starch and starch esters compressed at 174 MPa.

3.7. Microhardness and yield pressure parameters

From the results in Tables 1 and 4, it appears that for all three starches the yield pressure parameters follow the same trend as microhardness. Their relationship is examined in Fig. 7 by plotting microhardness against yield pressures derived from the four compression models. In all cases microhardness increased with yield pressure, which agrees with previously published results (Robert and Rowe, 1987; Egart et al., 2014, Alderborn 2003; Govedarica et al., 2015). Furthermore, the correlation between microhardness and tablet strength is tested in subfigure Fig. 7e. It shows that tensile strength is greater for SA with intermediate hardness, but lower for SN and SP with high and low microhardness respectively (Table 1). These results are in agreement with those of Cao et al. (2010) using a wide range of pharmaceutical materials. The conclusion from the plots in Fig. 7e is that there is no direct relationship between tablet strength and microhardness, and hence other factors should influence strength, besides microstructure.

Additionally, the function $f_{(E,Py)}$ relating elastic modulus and Heckel yield pressure was calculated for each starch using Eq. (22) (Roberts and Rowe, 1987).

$$f_{(EPy)} = 0.07 + 0.6\ln\left(\frac{E}{Yield\ pressure}\right) \quad (22)$$

For SA and SP the $f_{(E,Py)}$ values were 2.015 and 1.909, indicating elastic materials able to accommodate plastic strain, whereas for SN it was higher, 2.382 indicating behavior between elastic and rigid plastic solid. The above are in agreement with the reported elastoplasticity of maize starch (Roberts and Rowe 1987; Paronen and Juslin 1983).

3.8. Microstructure (SEM)

Plastic deformation should be reflected in the surface morphology of the tablets. In Fig. 8 representative SEM microphotographs of the upper tablet surface of the three starches compressed at 174 MPa are presented. Distinct boundaries appear to exist between the deformed native starch (SN) particles, whereas less distinct or no visible boundaries are seen between the particles of starch esters (SA, SP), indicating greater deformation and smoother tablet surface. This is explained by the greater plasticity of the esters, as indicated by their lower microhardness and yield pressure parameters (Tables 1, 4) (Korhonen et al., 2000; Raatikainen et al., 2002).

3.9. Estimation of tablet tensile strength using Hiestand's bonding index equation

During formulation work, it is useful to know the mechanical characteristics of produced tablets, and the importance of tablet tensile strength has been highlighted in the USP35 Chapter 1217 (2012). In this context, Hiestand's equation is a useful approach, connecting tablet strength with fundamental mechanical properties such as

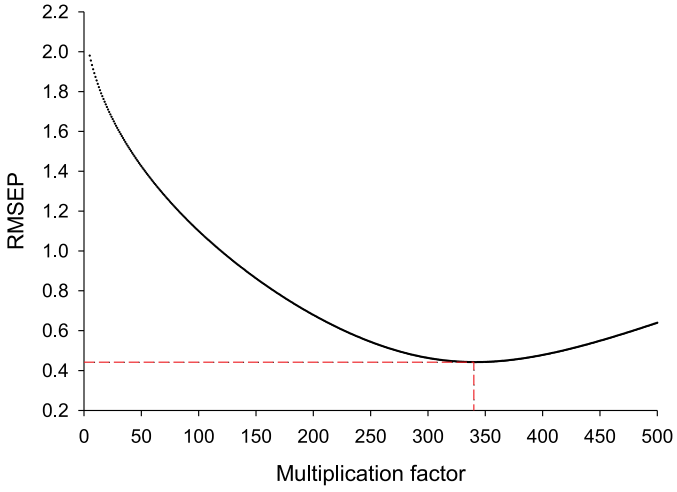

Fig. 9. Results of iteration process to find multiplication factor that minimized the root mean square error between calculated and experimental tablet strength.

Table 5
Parameters used in Hiestand's Eq. (21) for the calculation of tablet strength and calculated values (σ_T) using yield pressure parameters from compression models as 'effective compression pressure'

Starch type	*Pressure* (MPa)	p_F	σ_{T_Py} ($P' = Py$)	$\sigma_{T\_1/CKL}$ ($P' = 1/C_{KL}$)	$\sigma_{T\_1/b}$ ($P' = 1/b$)	$\sigma_{T\_\tau o'}$ ($P' = \tau_o'$)	σ_{T_exp}	Deviation of σ_{To}' from σ_{T_exp} (%)
SN	104	0.81	1.24	1.42	1.79	1.86	1.18	57.6
SN	139	0.87	1.27	1.46	1.83	1.91	1.28	49.2
SN	174	0.91	1.30	1.49	1.87	1.94	1.62	20.0
SA	104	0.77	1.88	2.02	1.67	2.39	2.60	8.2
SA	139	0.81	1.91	2.05	1.70	2.43	2.93	17.2
SA	174	0.83	1.93	2.07	1.71	2.45	3.00	18.5
SP	104	0.85	2.79	2.84	2.56	2.28	1.97	15.8
SP	139	0.89	2.83	2.89	2.60	2.32	2.12	8.1
SP	174	0.90	2.85	2.90	2.61	2.33	2.59	9.9

p_F: solid fraction; σ_{T_Py}, $\sigma_{T\_1/CKL}$ $\sigma_{T\_1/b}$, and $\sigma_{T\_\tau o'}$ tablet strength calculated using Heckel, K-L, Kawakita and Adams yield pressure respectively (calculated values were multiplied: for σ_{T_Py} by 40, for $\sigma_{T\_1/CKL}$ by 8, for $\sigma_{T\_1/b}$ by 500 and for τ_o' by 340); σ_{T_exp} experimental tablet strength

microhardness, effective pressure for particle deformation, elastic modulus, and also with interparticle surface forces which in the absence of solid bridges control bonding (Fichter et al. 2008). It also accounts for particle arrangement expressed by solid fraction, coordination number and particle size. Therefore, Eq. (21) was applied to derive a tablet strength equation describing the results of all three starches using values of particle radii, microhardness (Table 1), ξi (0.06, 0.04 and 0.03 for SN, SA and SP respectively calculated from the elastic moduli in Table 1) and dispersive forces (Table 2). A modification in the equation was made to allow substitution of the effective pressure for particle deformation (P', Eq. (21)) with one of the yield pressure parameters: Py (calculated strength denoted σ_{T_Py}) $1/C_{KL}$ ($\sigma_{T\_1/CKL}$), $1/b$ ($\sigma_{T\_1/b}$,) and τ_o' ($\sigma_{T\_\tau o'}$). A further modification was to use as coordination number $N = 15$ obtained from Eq. (23) (Ouchiyama and Tanaka 1981) assuming uniform spherical particles packed at p_F 0.85.

$$N = 2.5[7 - 8(1 - p_F)] \quad (23)$$

Despite the two modifications applied, the calculated tablet strengths were found to be orders of magnitude lower that the experimental. For this reason, iteration was applied to find multiplication factors that minimized the Root Mean Square Error (Fig. 9). These were respectively x40 for σ_{T_Py}, x8 for $\sigma_{T\_1/CKL}$, x500 for $\sigma_{T\_1/b}$ and x340 for $\sigma_{T\_\tau o'}$.

In Table 5 calculated (σ_{T_Py}, $\sigma_{T\_1/CKL}$, $\sigma_{T\_1/b}$, $\sigma_{T\_\tau o'}$) and experimental (σ_{Texp}) tablet strength values for different compression pressures and corresponding solid fractions are presented and plots of calculated

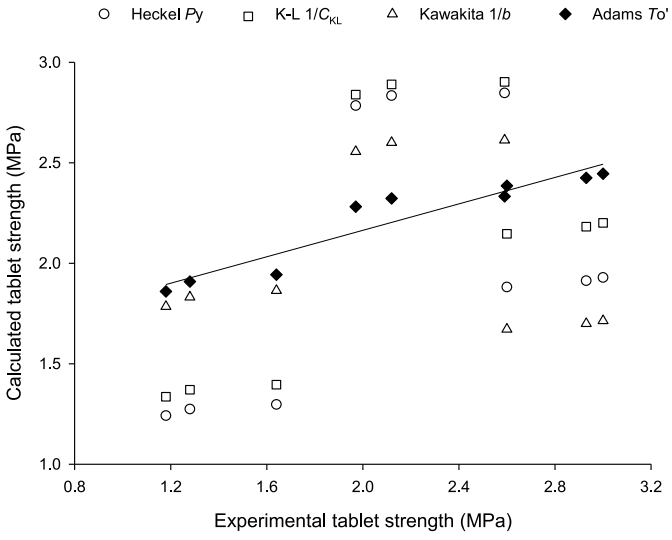

Fig. 10. Plots of tensile strength calculated from the modified Hiestand equation using yield pressure parameters from compression models as the 'effective compression pressure' against experimental strength values.

against experimental strength are shown in Fig. 10. From the last it can be seen that only when τ_o' was substituted in Eq. (21) a single straight line ($R^2 = 0.902$) accommodating the results of all three starches was obtained. Substitution of the other yield pressure parameters gave straight lines only for a certain starch powder (Sun et al., 2018). The ability of Adams parameter τ_o' to provide satisfactory substitution in Hiestand's equation should be due to its correlation with the single particle strength (Adams and McKeown 1996). A drawback of Adams model is that it neglects the elastic energy stored during compaction, which in the case of starch powders is considerable as indicated by the high elastic recovery values of 11.6%, 12.7% and 12.2% for SN, SA and SP respectively (Table 1). However, since these values are not very different, elasticity should not affect the correlation between calculated and experimental strength. Furthermore, in Table 5 deviations between calculated using τ_o' and experimental strength values are presented and they vary between 8.0% and 57.6%.

On the basis of the above results it can be concluded that the predicting ability of the modified Hiestand's equation is rather low, and in view of other important factors such as presence of disintegrants and lubricants, its applicability to real tablet formulations requires further substantiation. The deviations of the theoretical from the experimental values are ascribed mainly to two reasons. One is plastic or viscoelastic deformation resulting in greater curvature of contacting interparticle surfaces during decompression and greater contact area. Viscoelastic behavior is manifested in the Heckel plot (Fig. 6a) as continued increase of densification after force removal. A second reason is that since the compaction and mechanical strength of starch is affected by the moisture content, non-dispersive forces and in particular H-bonding cannot be overlooked (Dave et al., 2015). This point is supported by the thermograms in Fig. 3, showing significant water loss at low temperatures of about 40–45 °C, suggesting that besides any internally absorbed moisture, a significant part is externally adsorbed water and could be responsible for H-bonding (Malamataris et al., 1991; Dave et al., 2015). Another reason may be that plasticity parameters obtained by model fitting using 'in-die' data (as in this work) may impart some error due to the elastic deformation of particles under pressure.

4. Conclusions

The lower crystallinity of acetate and propionate starch esters compared to native starch resulted in lower microhardness, modulus of elasticity and greater deformation during compaction. Correlation was established between microhardness or modulus of elasticity with yield pressure parameters obtained from different models of powder compaction, confirming their strong connection. Calculated tensile strength on the basis of Hiestand's equation modified by replacing the 'effective compression pressure' with the Adams parameter τ_o' correlated well ($R^2 = 0.903$) with experimental values and described all starch powders, and thus providing a possible tool to formulators during product development. Further experiments are needed to show that this idea

will work in practice on a real tablet formulation with disintegrants and lubricants.

Funding

This work received financial support from the Research Council, The Hashemite University, Zarqa–Jordan.

Acknowledgment

The authors acknowledge the technical assistance of Frederik Fleissner and Mihaela Dubuisson (Anton Paar, Austria) in conducting Raman spectroscopy and nanoindentation tests. Authors are also immensely grateful to the reviewers for their comments.

Supplementary materials

Supplementary material associated with this article can be found, in the online version, at doi:10.1016/j.ejps.2020.105292.

References

Adams, M.J., McKeown, R., 1996. Micromechanical analyses of the pressure-volume relationships for powders under confined uniaxial compression. Powder Technol. 88, 155–163.
Akin-Ajani, O.D., Itiola, O.A., Odeku, O.A., 2014. Effect of acid modification on the material and compaction properties of fonio and sweet potato starches. Starke 66, 749–759.
Alderborn, G., 2003. A novel approach to derive a compression parameter indicating effective particle deformability. Pharm. Dev. Technol. 8 (4), 367–377.
Almeida, M.R., Alves, R.S., Nascimbem, L.B.L.R., Stephani, R., Poppi, R.J., de Oliveira, L.F.C., 2010. Determination of amylose content in starch using Raman spectroscopy and multivariate calibration analysis. Anal. Bioanal. Chem. 397, 2693–2701.
Ameye, D., Voorspoels, J., Foreman, P., Tsai, J., Richardson, P., Geresh, S., Remon, J.P., 2001. Trypsin inhibition, calcium and zinc ion binding of starch–g-poly (acrylic acid) copolymers and starch/poly (acrylic acid) mixtures for peroral peptide drug delivery. J. Control. Rel. 75, 357–364.
Avgerinos, T., Kantiranis, N., Panagopoulou, A., Malamataris, S., Kachrimanis, K, Nikolakakis, I, 2018. Mechanical properties and drug release of venlafaxine HCl solid mini matrices prepared by hot-melt extrusion and hot or ambient compression. Drug Dev. Ind. Pharm. 44, 338–348.
Buckton, G., Newton, J.M., 1986. Assessment of the wettability of powders by use of compressed powder discs. Powder Technol. 46, 201–208.
Buléon, A, Colonna, P, Planchot, V, Ball, S, 1998. Starch granules: structure and biosynthesis. Int. J. Biol. Macromol. 23, 85–112.
Cao, X., Morganti, M., Hancock, B.C., Masterson, V.M., 2010. Correlating particle hardness with powder compaction performance. J. Pharm. Sci. 99, 4307–4316.
Cespi, M., Perinelli, D.R., Casettari, L., Bonacucina, G., Caporicci, G., Rendina, F., Palmieri, G.F., 2014. Use of in-die powder densification parameters in the implementation of process analytical technologies for tablet production on industrial scale. Int. J. Pharm. 477, 140–147.
Dave, S.V., Chanda, M., Sayles, M., Popielarczyk, M., Boyce, H., Bompelliwar, S.K., Bates, S., Morris, K.R., Haware, R.V., 2015. Correlation of structural and macroscopic properties of starches, with their tabletability using the SM2 approach. J. Pharm. Sci. 104, 3870–3882.
Denny, P.J., 2002. Compaction equations: a comparison of the Heckel and Kawakita equations. Powder Technol. 127, 162–172.
Diop, C.I.K., Li, H.L., Xie, B.J., Shi, J., 2011. Effects of acetic acid/acetic anhydride ratios on the properties of corn starch acetates. Food Chem. 126, 1662–1669.
Egart, M., Ilić, I., Janković, B., Lah, N., Srčič, S., 2014. Compaction properties of crystalline pharmaceutical ingredients according to the Walker model and nanomechanical attributes. Int. J. Pharm. 472, 347–355.
Fell, J.T., Newton, J.M., 1970. Determination of tablet strength by the diametral-compression test. J. Pharm. Sci. 59, 688–691.
Feng, J., Grant, D., Sun, C.C., 2007. Influence of crystal structure on the tableting properties of n-alkyl 4-hydroxybenzoate esters (Parabens). J. Pharm. Sci. 96 (12), 3324–3333.
Fichtner, F., Mahlin, D., Welch, K., Gaisford, S., Alderborn, G., 2008. Effect of surface energy on powder compactibility. Pharm. Res. 25 (12), 2750–2759.
Govedarica, B., Ilija Ilić, I., Šibanc, R., Dreu, R., Srčič, S., 2012. The use of single particle mechanical properties for predicting the compressibility of pharmaceutical materials. Powder Technol. 225, 43–51.
Heckel, R.W., 1961. Density-pressure relationships in powder compaction. Trans. Metall. Soc. AIME 221, 671–675.
Heertjes, P.M., Kossen, N.W.F., 1967. Measuring the contact angles of powder-liquid systems. Powder Technol. 1 (1), 33–42.
Heng, J.Y.Y., Pearse, D.F., Thielmann, F., Lampke, T., Bismarck, A., 2007. Methods to determine surface energies of natural fibres: a review. Compos. Interfaces 14 (7–9), 581–604.
Hiestand, E.N., 1985. Dispersion forces and plastic deformation in tablet bond. J. Pharm. Sci. 74, 768–770.
Holm, R., Borkenfelt, S., Allesø, M., Andersen, J.E.T., Beato, S., Holm, P., 2016. Investigation of surface porosity measurements and compaction pressure as means to ensure consistent contact angle determinations. Int. J. Pharm. 498, 355–361.
Hong, L.F., Cheng, L.H., Lee, C.W, Peh, K.K, 2015. Propionylated corn starch and its application as stabiliser. Food Technol. Biotechnol. 53 (3), 278–285.
Katz, J.M., Buckner, I.S., 2013. Characterization of strain rate sensitivity in pharmaceutical materials using indentation creep analysis. Int. J. Pharm 442, 13–19.
Kawakita, K., Lüdde, K.H., 1971. Some considerations on powder compression equations. Powder Technol. 4, 61–68.
Korhonen, O., Raatikainen, P., Harjunen, P., Nakari, J., Suihko, E., Peltonen, S., Paronen, P., 2000. Starch acetates—multifunctional direct compression excipients. Pharm. Res 17, 1138–1143.
Kuentz, M., Leuenberger, H., 1999. Pressure susceptibility of polymer tablets as a critical property: a modified Heckel equation. J. Pharm. Sci. 88 (2), 174–179.
Kung, C.H., Sow, P.K., Zahiri, B., Mérida, W., 2019. Assessment and interpretation of surface wettability based on sessile droplet contact angle measurement: challenges and opportunities. Adv. Mater. Interfaces 6 1900839.
Lamešić, D., Planinšek, O., Ilić, G.I., 2018. Modified equation for particle bonding area and strength with inclusion of powder fragmentation propensity. Eur. J. Pharm. Sci. 121, 218–227.
Lerk, C.F., Schoonen, A.J.M., Fell, J.T., 1976. Contact angles and wetting of pharmaceutical powders. J. Pharm. Sci. 65 (6), 843–847.
Mäki, R., Suihko, E., Korhonen, O., Pitkänen, H., Niemi, R., Lehtonen, M., Ketolainen, J., 2006. Controlled release of saccharides from matrix tablets. Eur. J. Pharm. Biopharm. 62 (2), 163–170.
Malamataris, S., Goidas, P., Dimitriou, A., 1991. Moisture sorption and tensile strength of some tableted direct compression excipients. Int. J. Pharm. 68, 51–60.
Masterson, M.V., Cao, X., 2008. Evaluating particle hardness of pharmaceutical solids using AFM nanoindentation. Int. J. Pharm. 362, 163–171.
Nikolakakis, I., Pilpel, N., 1988. Effects of particle shape and size on the tensile strengths of powders. Powd. Technol. 56, 95–103.
Nyström, C., Alderborn, G., Duberg, M., Per-Gunnar Karehill, P-G., 1993. Bonding surface area and bonding mechanism-two important factors for the understanding of powder compactability. Drug Dev. Ind. Pharm. 19, 2143–2196.
Odeku, O.A., Picker-Freyer, K.M., 2009. Characterization of acid modified dioscorea starches as direct compression excipient. Pharm. Dev. Technol. 14, 259–270.
Oliver, W.C., Pharr, G.M., 2004. Measurement of hardness and elastic modulus by instrumented indentation: advances in understanding and refinements to methodology. J. Mater. Res. 19 (1), 3–20.
Ouchiyama, N., Tanaka, T., 1981. Porosity of a mass of solid particles having a range of sizes. Ind. Eng. Chem. Fundam. 20, 66–71.
Paronen, P., Juslin, M., 1983. Compressional characteristics of four starches. J. Pharm. Pharmacol. 35 (10), 627–635.
Patel, S., Kaushal, A.M., Bansal, A.K., 2010. Mechanistic investigation on pressure dependency of Heckel parameter. Int. J. Pharm. 389, 66–73.
Paul, S., Sun, C.C., 2017. The suitability of common compressibility equations for characterizing plasticity of diverse powders. Int. J. Pharm. 532 (1), 124–130 2017,.
Pereira, D.C., de Faria, D.L.A., Constantino, V.R.L., 2006. Cu^{II} hydroxy salts: characterization of layered compounds by vibrational spectroscopy. J. Braz. Chem. Soc. 17, 1651–1657.
Perez, S., Bertoft, E., 2010. The molecular structures of starch components and their contribution to the architecture of starch granules: a comprehensive review. Starke 62, 389–420.
Picker-Freyer, K.M., Liao, X., Zhang, G., Wiedmann, T.S., 2007. Evaluation of the compaction of sulfathiazole polymorphs. J. Pharm. Sci. 96, 2111–2124.
Pohja, S., Suihko, E., Vidgren, M., Paronen, P., Ketolainen, J., 2004. Starch acetate as a tablet matrix for sustained drug release. J. Control. Release 94 (2), 293–302.
Raatikainen, P., Korhonen, O., Peltonen, S., Paronen, P., 2002. Acetylation enhances the tabletting properties of starch. Drug Dev. Ind. Pharm. 28 (2), 165–175.
Roberts, R., Rowe, R.C., 1987. The compaction of pharmaceutical and other model materials – a pragmatic approach. Chem. Eng. Sci. 42, 903–911.
Sakhnini, N., Al-Zoubi, N., Al-Obaidi, G.H., Ardakani, A., 2015. Sustained release matrix tablets prepared from cospray dried mixtures with starch hydrophobic esters. Die Pharm. 70 (3), 177–182.
Singh, A.V., Nath, L.K., 2012a. Evaluation of acrylamide grafted moth bean starch as controlled release excipient. Carbohydr. Polym. 87 (4), 2677–2682.
Singh, A.V., Nath, L.K., 2012b. Evaluation of acetylated moth bean starch as a carrier for controlled drug delivery. Int. J. Biol. Macromol. 50 (2), 362–368.
Singh, A.V., Nath, L.K., 2013a. Formulation development and evaluation of lamivudine controlled release tablets using cross-linked sago starch. Expert Opin. Drug Deliv. 10 (2), 173–182.
Singh, A.V., Nath, L.K., 2013b. Evaluation of microwave assisted grafted sago starch as controlled release polymeric carrier. Int. J. Biol. Macromol. 60, 62–68.
Singh, A.V., Nath, L.K., 2013c. Evaluation of chemically modified hydrophobic sago starch as a carrier for controlled drug delivery. Saudi Pharm. J. 21 (2), 193–200.
Sun, C.C., 2004. A novel method for deriving true density of pharmaceutical solids including hydrates and water-containing powders. J. Pharm. Sci. 93 (3), 646–653.
Sun, W-J., Kothari, S., Sun, C.C., 2018. The relationship among tensile strength, Young's modulus, and indentation hardness of pharmaceutical compacts. Powder Technol. 331, 1–6.
The United States Pharmacopoeial Convention, May 2012. Chapter 1217 Tablet Breaking Force.
Tuovinen, L., Peltonen, S., Liikola, M., Hotakainen, M., Lahtela-Kakkonen, M., Poso, A., Järvinen, K., 2004. Drug release from starch-acetate microparticles and films with

and without incorporated α-amylase. Biomaterials 25 (18), 4355–4362.
Van Veen, B., Pajander, J., Zuurman, K., Lappalainen, R., Poso, A., Frijlink, H.W., Ketolainen, J., 2005. The effect of powder blend and tablet structure on drug release mechanisms of hydrophobic starch acetate matrix tablets. Eur. J. Pharm. Biopharm. 61 (3), 149–157.
Wöhl-Bruhn, S., Bertz, A., Harling, S., Menzel, H., Bunjes, H., 2012. Hydroxyethyl starch-based polymers for the controlled release of biomacromolecules from hydrogel microspheres. Eur. J. Pharm. Biopharm. 81 (3), 573–581.
Wu, S., 1971. Calculation of interfacial tension in polymer systems. J. Polym. Sci. C Polym. Symp. 34, 19–30.
Yang, B.Y., Montgomery, R., 2008. Preparation and physical properties of starch mixed esters. Starke 60 (3-4), 146–158.
Yap, S.F., Adams, M.J., Seville, J.P., Zhang, Z., 2008. Single and bulk compression of pharmaceutical excipients: evaluation of mechanical properties. Powder Technol. 185, 1–10.
Zhu, J.F., Zhang, J.H., Lai, Z.C., Zhang, G.H., 2007. Synthesis and characterization of maize starch acetates and its biodegradable film. Polym. Plast. Technol. Eng. 46, 1135–1141.
Zografi, G., Tam, S.S., 1976. Wettability of pharmaceutical solids: estimates of solid surface polarity. J. Pharm. Sci 65 (8), 1145–1149.